Energy Materials

Supplementary Material

High-entropy nitrides from dual entropic and enthalpic forces for high-efficiency oxygen evolution reaction

Jingyun Jiang[1], Yifan Xu[2], Zheng Wang[1], Hongbo Zhang[1], Qun Xu[1,3,*], Yuanjian Li[4,*]

[1]College of Materials Science and Engineering, Zhengzhou University, Zhengzhou 450052, Henan, China.
[2]School of Materials Science and Engineering, Nanyang Technological University, Singapore 639798, Singapore.
[3]Henan Institute of Advanced Technology, Zhengzhou University, Zhengzhou 450052, Henan, China.
[4]Institute of Materials Research and Engineering (IMRE), Agency for Science, Technology and Research (A*STAR), Singapore 138634, Singapore.

***Correspondence to:** Prof. Qun Xu, College of Materials Science and Engineering, Zhengzhou University, No. 100 Science Avenue, Zhengzhou 450052, Henan, China; Henan Institute of Advanced Technology, Zhengzhou University, No. 100 Science Avenue, Zhengzhou 450052, Henan, China. E-mail: qunxu@zzu.edu.cn; Dr. Yuanjian Li, Institute of Materials Research and Engineering (IMRE), Agency for Science, Technology and Research (A*STAR), 2 Fusionopolis Way, Singapore 138634, Singapore. E-mail: li_yuanjian@imre.a-star.edu.sg

Supplementary Figures and Tables

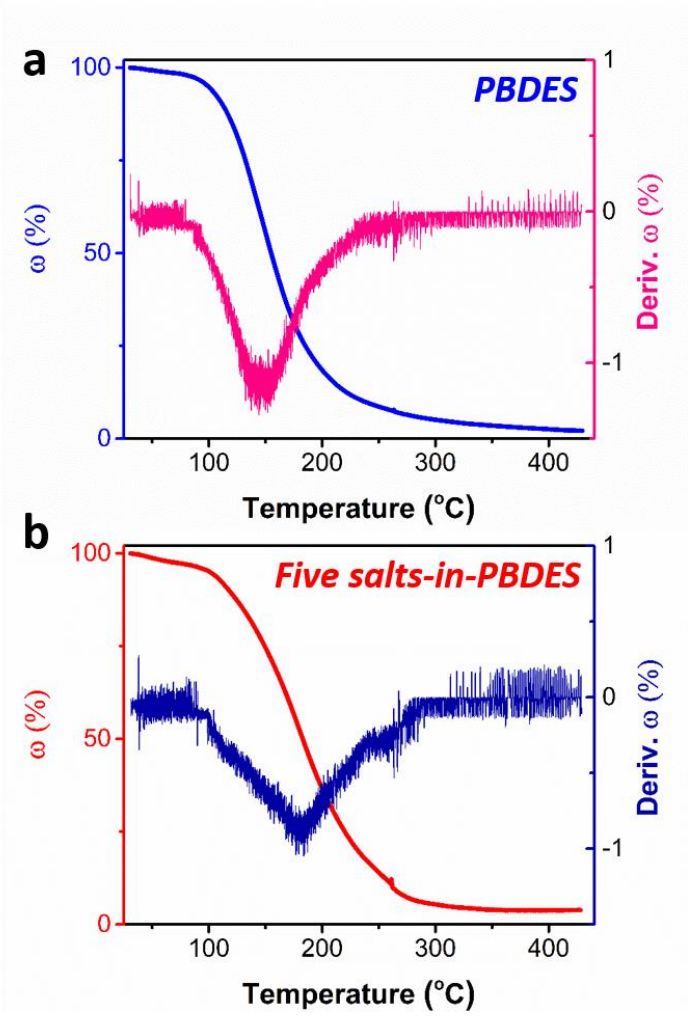

Figure S1 TGA and DTG curves of PBDES with (b) or without (a) metal salts from 30 to 430 °C at a heating rate of 3 °C min^{-1}.

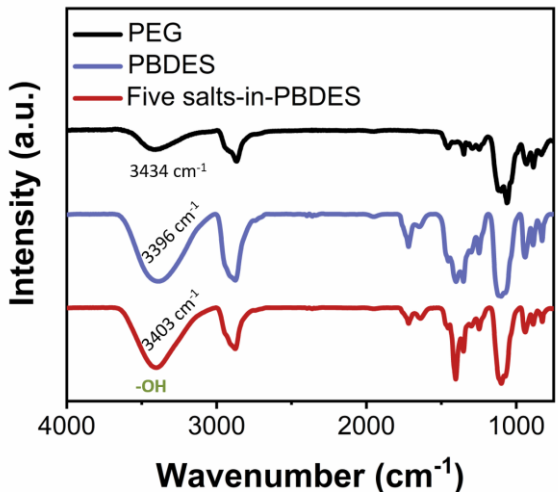

Figure S2 FT-IR spectrum of PEG (black), PBDES (blue) and salts-in-PBDESs (red) ranging from 4000 to 750 cm^{-1}.

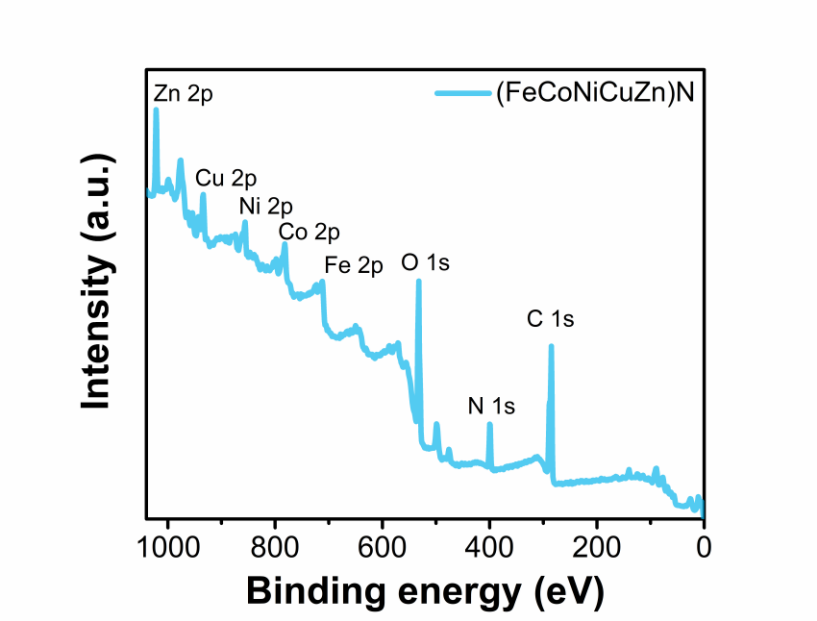

Figure S3 XPS survey spectra of (FeCoNiCuZn)N.

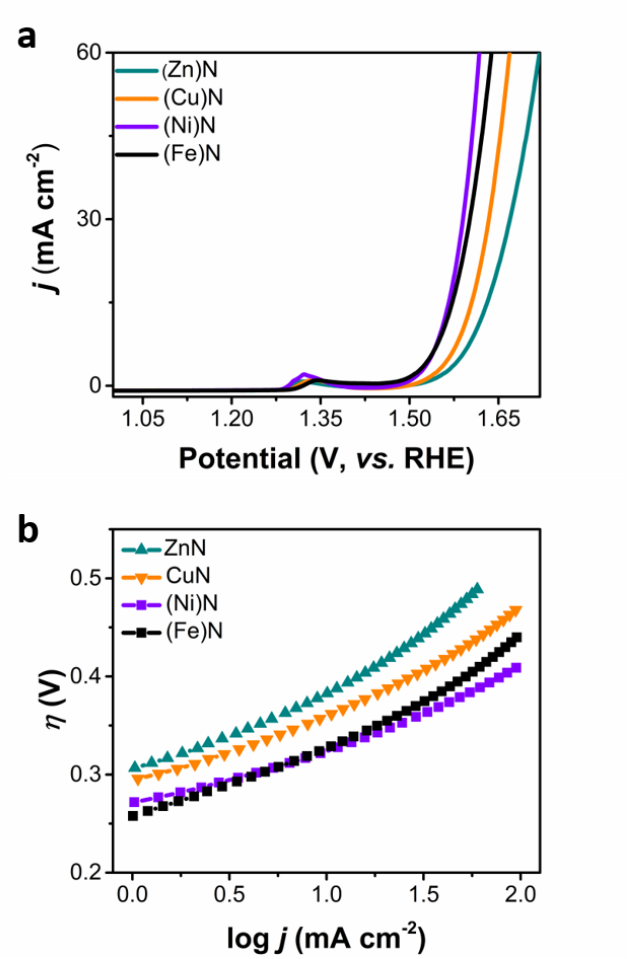

Figure S4 Electrochemical performance of the obtained samples. (a)LSV curves and (b) the related Tafel plots (Inset of a) of (Fe)N, (Ni)N, (Cu)N and (Zn)N.

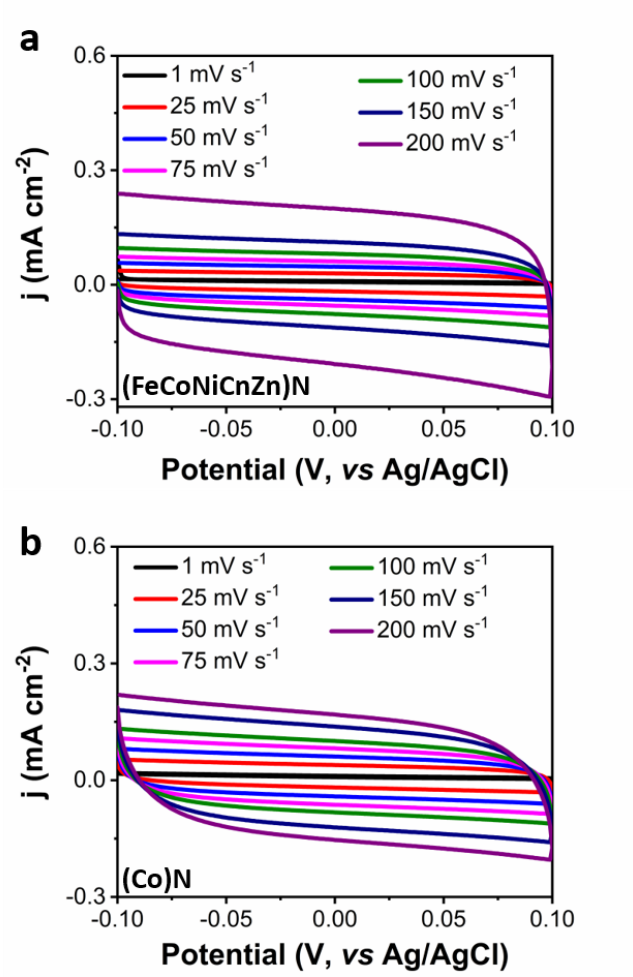

Figure S5 Cyclic voltammograms taken over a range of scan rates from 1 to 200 mV s^{-1} for (FeCoNiCuZn)N (a) and (Co)N (b).

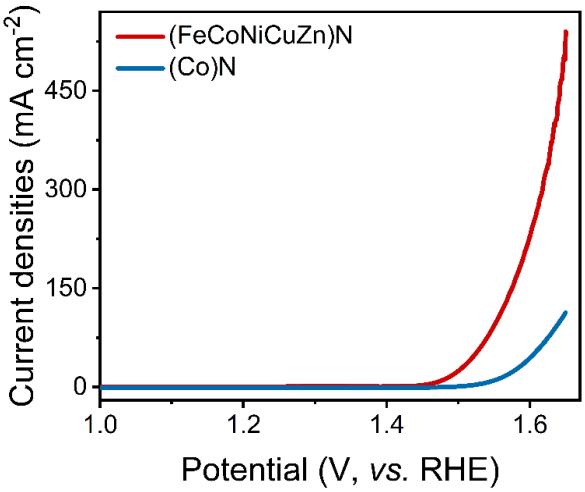

Figure S6 ECSA-normalized LSV curves of the obtained samples-modified GC electrodes.

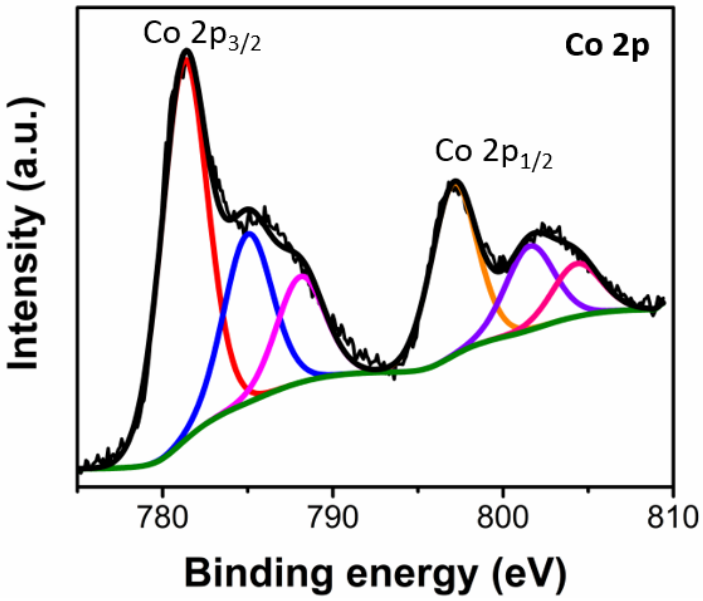

Figure S7 The Co 2p spectra of (Co)N.

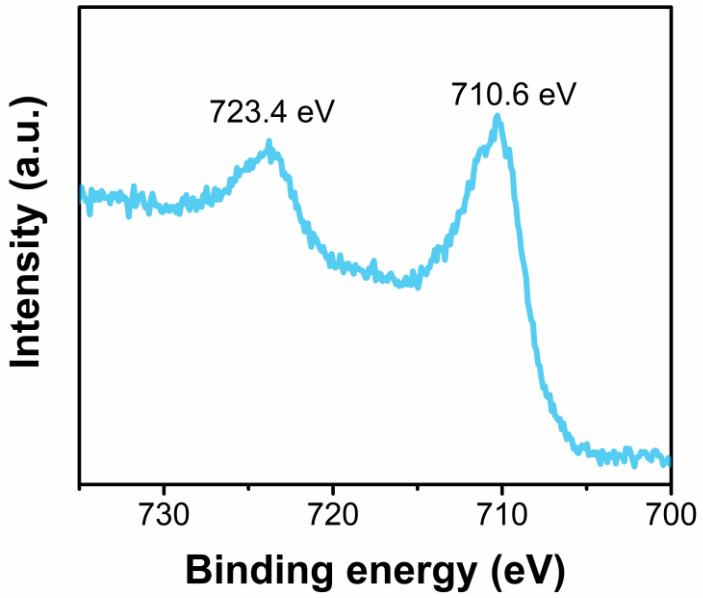

Figure S8 The Fe 2p spectra of (Fe)N.

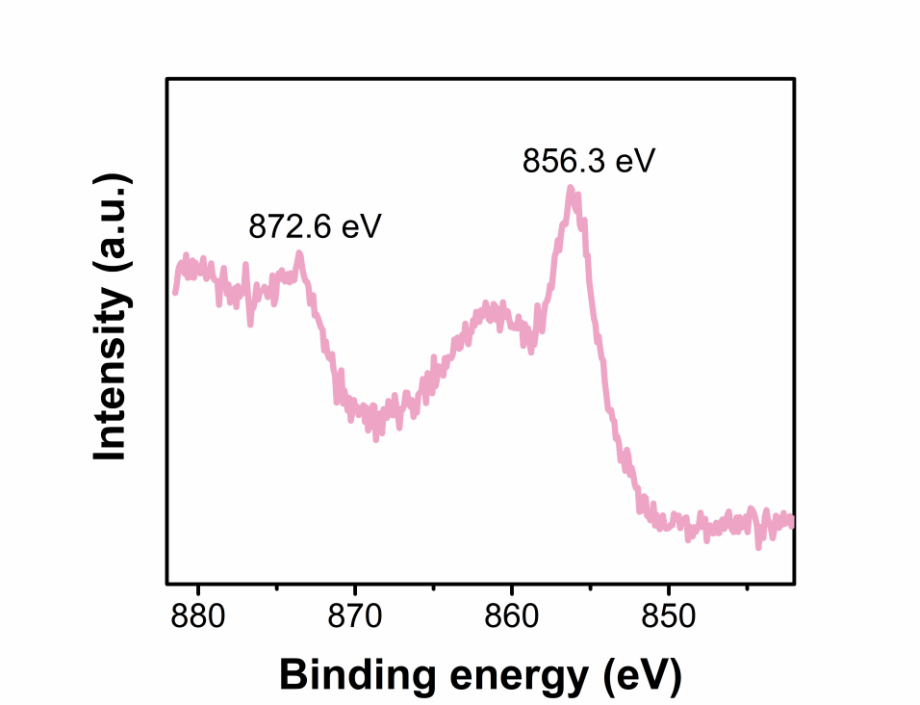

Figure S9 The Ni 2p spectra of (Ni)N.

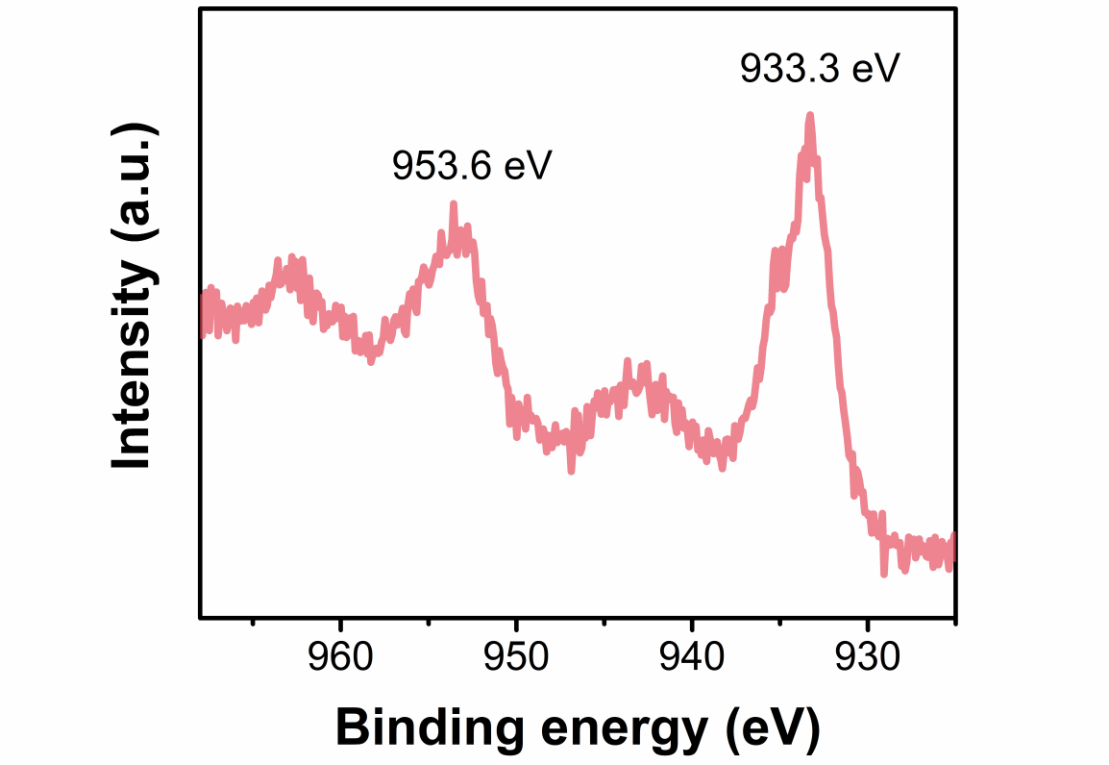

Figure S10 The Cu 2p spectra of (Cu)N.

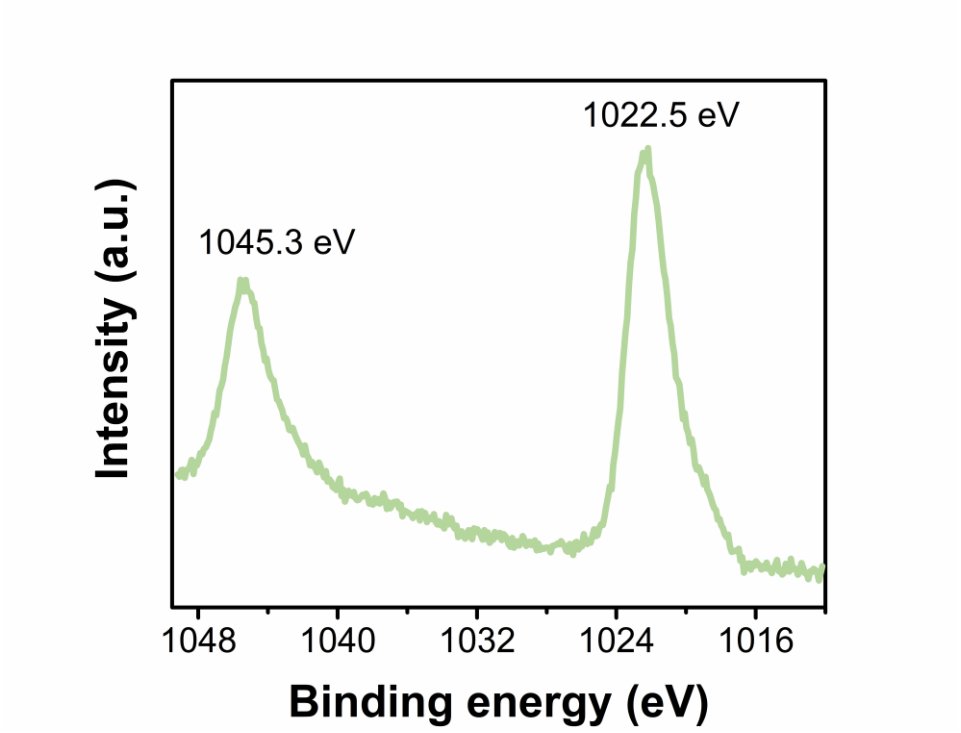

Figure S11 The Zn 2p spectra of (Zn)N.

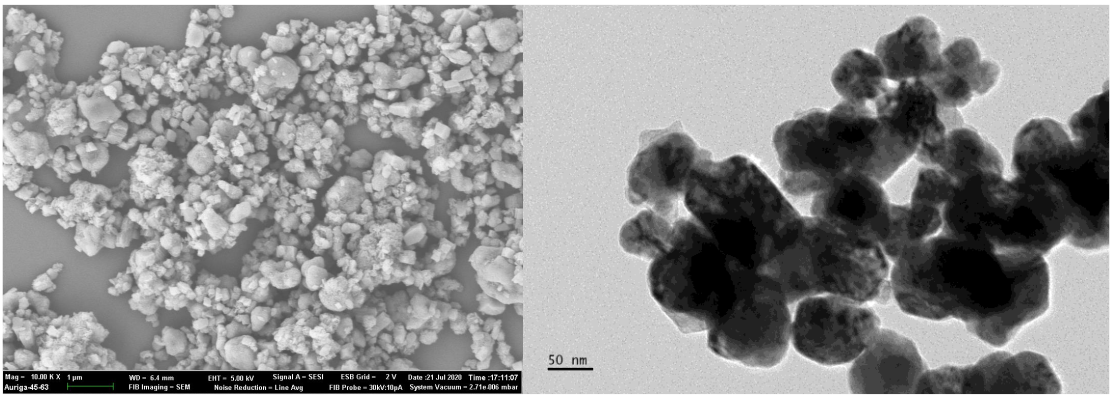

Figure S12 SEM and TEM images of (FeCoNiCuZn)N after long-term stability.

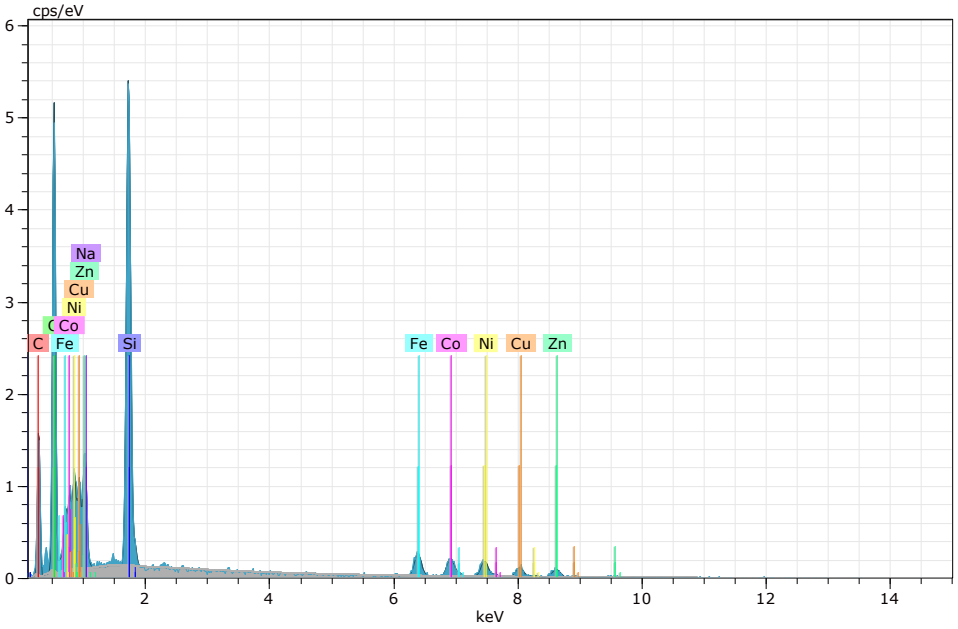

Figure S13 EDS analysis of (FeCoNiCuZn)N after long-term stability.

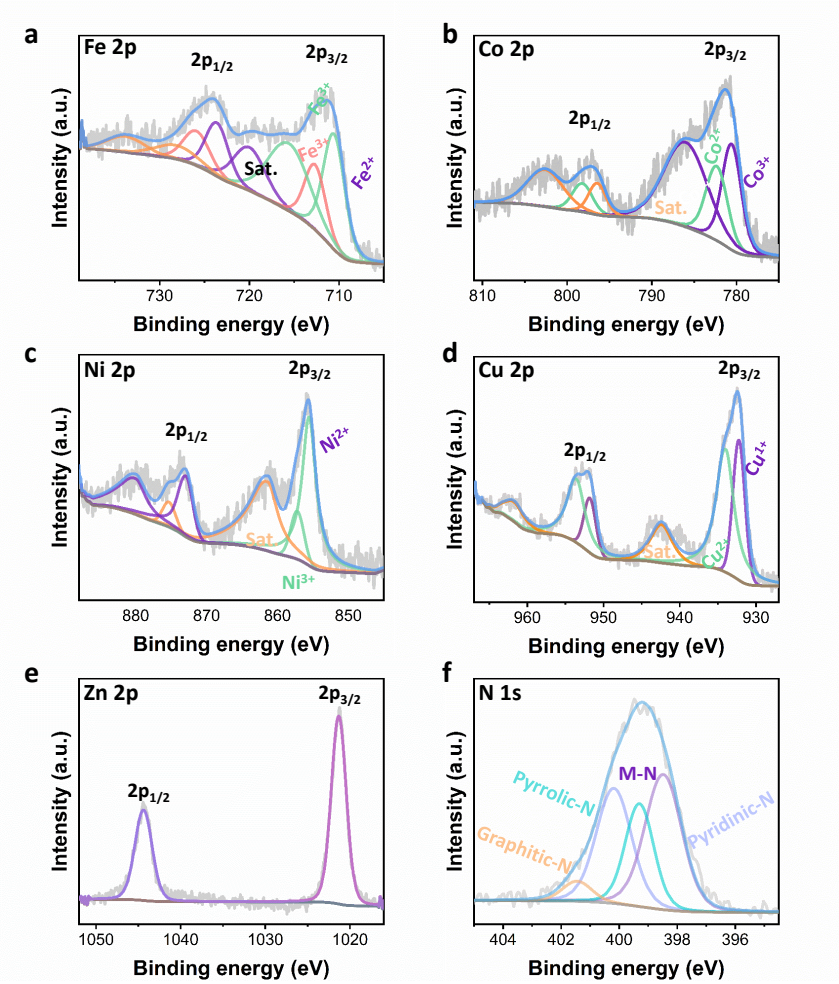

Figure S14 XPS spectra of (FeCoNiCuZn)N after electrolysis: Fe (a), Co (b), Ni (c), Cu (d), Zn (e), and N (f).

Table S1. ICP analysis of (FeCoNiCuZn)N.

Samples	Contents (ppm)				
	Fe	**Co**	**Ni**	**Cu**	**Zn**
(FeCoNiCuZn)N	38.87	40.05	36.98	50.01	37.99

Table S2. Comparison of electrochemical OER parameters of various catalysts.

Samples	**Overpotential @10 mA cm^{-2}**	**Tafel slope (mV dec^{-1})**	***Reference***
(FeCoNiCuZn)N	223	57	**Our work**
(Co)N	340	68	**Our work**
Co/Co_4N@NC	262	130	*J. Mater. Chem. A*, 2024[1]
Fe_2P/Ni_3N	180	45.5	*Small*, 2023[2]
$(CrMnFeCoNi)S_x$	295@100	66	*Adv. Energy Mater.*, 2020[3]
NiMoN/NiFe LDH	236@500	42.2	*Nat. Commun.*, 2023[4]
FeNiCoCrMn-G	229	40	*Adv. Sci.*, 2021[5]
$NiFe_{0.05}$-N-$Cl_{0.5}(NO_3)_{0.5}$-CP	298@100	50	*New J. Chem.* 2024[6]
$(Fe_{0.2}Co_{0.2}Ni_{0.2}Cu_{0.2}Zn_{0.2})Al_2O_4$	430	-	*J. Am. Chem. Soc.*, 2023[7]
$Fe_{0.3}Ni_1Co_2$/S-C	276	52.2	*J. Alloy. Compd.*, 2024[8]
CoCuSrCe	290	42	*Dalton Trans.*, 2024[9]
NiFeCoZn/NiZn-Ni/NF-24h	266@50	56.12	*Chinese J. Chem.*, 2024[10]
FeNi@FeNiB-700	272	89	*J. Mater. Chem. A*, 2019[11]
Fe/Fe_3C-modified Carbon	320	51	*Angew. Chem. Eng. In.*, 2021[12]
Cu-CoOOH@CFP	227	73.3	*Chem. Eng. J.*, 2021[13]

2D Co_2N@CoNC-IN-CP	217	66	*Adv. Energy Mater.*, 2020[14]

Table S3. EXAFS data fitting results of Co K-edge curves from (FeCoNiCuZn)N and (Co)N samples (S_0^2 = 0.87). S_0^2 is the amplitude reduction factor according to the experimental EXAFS fit of Co foil; CN is the coordination number; R is interatomic distance (the bond length between central atoms and surrounding coordination atoms); σ^2 is Debye-Waller factor (a measure of thermal and static disorder in absorber-scatterer distances); ΔE_0 is edge-energy shift (the difference between the zero kinetic energy value of the sample and that of the theoretical model); R factor is used to value the goodness of the fitting.

Sample	**Path**	**CN**	***R* (Å)**	σ^2	ΔE_o	***R factor***
(FeCoNiCuZn)N	Co-N	7.55±0.91	2.10±0.01	0.0089	-2.56±1.48	0.006
(Co)N	Co-N	6.38±0.81	2.09±0.01	0.0079	-5.70±1.55	0.005

Reference

1. Choi, H. W., Kim, J., Bang, H.-S., et al. Tracking accelerated oxygen evolution reaction enabled by explosive reconstruction of active species based on Co_xN@NC. *J. Mater. Chem. A* 2024; 12: 7067-79. [DOI: 10.1039/d4ta00196f]
2. Ma, W., Li, D., Liao, L., et al. High-performance bifunctional porous iron-rich phosphide/nickel nitride heterostructures for alkaline seawater splitting. *Small* 2023; 19: 2207082. [DOI: 10.1002/smll.202207082]
3. Cui, M., Yang, C., Li, B., et al. High-entropy metal sulfide nanoparticles promise high-performance oxygen evolution reaction. *Adv. Energy Mater. 2020*; 11: 2002887. [DOI: 10.1002/aenm.202002887]
4. Zhai, P., Wang, C., Zhao, Y., et al. Regulating electronic states of nitride/hydroxide to accelerate kinetics for oxygen evolution at large current density. *Nat. Commun.* 2023; 14: 1873. [DOI: 10.1038/s41467-023-37091-x]
5. Nguyen, T. X., Su, Y. H., Lin, C. C., Ruan, J., and Ting, J. M. A new high entropy glycerate for high performance oxygen evolution reaction. *Adv. Sci.* 2021; *8*: 2002446. [DOI: 10.1002/advs.202002446]
6. Wei, Y., Xu, Y., Zhang, H., Jiang, J., and Xu, Q. Anion-regulated 2D amorphous binary nickel–iron nitrides for efficient water oxidation at high-current-densities. *New J. Chem.* 2024; 48: 11206-10. [DOI: 10.1039/d4nj01886a]
7. Katzbaer, R. R., dos Santos Vieira, F. M., Dabo, I., Mao, Z., and Schaak, R. E. Band gap narrowing in a high-entropy spinel oxide semiconductor for enhanced oxygen evolution catalysis. *J. Am. Chem. Soc.* 2023; 145: 6753-61. [DOI: 10.1021/jacs.2c12887]

8. Hong, L., Liu, Z., Zhang, X., et al. Enhanced OER electrocatalyst performance by sulfur doping trimetallic compounds hybrid catalyst supported on reduced graphene oxide. *J. Alloys and Comp.* 2024; 991: 174238. [DOI: 10.1016/j.jallcom.2024.174238]
9. Roy, S., Dahiya, P., Mandal, T.K., and Roy, S.. The role of reducibility vis-à-vis oxygen vacancies of doped Co_3O_4/CeO_2 in the oxygen evolution reaction. *Dalton Trans.* 2024; 53: 5484-94. [DOI: 10.1039/d4dt00315b]
10. Zhang, Q., Wang, X., Jian, T., et al. Free-standing multiscale porous high entropy NiFeCoZn alloy as the highly active bifunctional electrocatalyst for alkaline water splitting. *Chin. J. Chem.* 2024; *42*: 1465-73. [DOI: 10.1002/cjoc.202300718]
11. Yuan, H., Wang, S., Gu, X., Tang, B., Li, J., and Wang, X. One-step solid-phase boronation to fabricate self-supported porous FeNiB/FeNi foam for efficient electrocatalytic oxygen evolution and overall water splitting. *J. Mater. Chem. A* 2019; 7:19554-64. [DOI: 10.1039/c9ta04076e]
12. Liang, X., Xiao, J., Weng, W., and Xiao, W. Electrochemical reduction of carbon dioxide and iron oxide in molten salts to Fe/Fe_3C modified carbon for electrocatalytic oxygen evolution. *Angew. Chem. Int. Ed.* 2020; 60: 2120-24. [DOI: 10.1002/anie.202013257]
13. Yan, L., Zhang, B., Liu, Z., and Zhu, J. Synergy of copper doping and oxygen vacancies in porous CoOOH nanoplates for efficient water oxidation. *Chem. Eng. J.* 2021; 405: 126198. [DOI: 10.1016/j.cej.2020.126198]
14. Jiang, J., Yan, P., Zhou, Y., et al. Interplanar growth of 2D non-Van der Waals Co_2N-based heterostructures for efficient overall water splitting. *Adv. Energy Mater*. 2020; 10: 2002214. [DOI: 10.1002/aenm.202002214]